Atmospheric Research 325 (2025) 108239

Contents lists available at ScienceDirect

Atmospheric Research

journal homepage: www.elsevier.com/locate/atmosres

Estimation of light absorption by secondary brown carbon during agricultural residues burning

B. Domínguez [a], J.F. Nicolás [b,*], E. Mantilla [a], C. Gimeno [a], E. Borrás [a], M. Ródenas [a], T. Vera [a], R. Soler [a], M. Alfosea-Simón [b], E. Yubero [b], J. Crespo [b], N. Galindo [b], A. Clemente [b], A. Muñoz [a,*]

[a] Fundación CEAM. C/Charles R. Darwin, 14. Parque Tecnológico, 46980 Paterna, Valencia, Spain
[b] Atmospheric Pollution Laboratory (LCA), Department of Applied Physics, Miguel Hernández University. Avenida de la Universidad S/N, 03202 Elche, Spain

ARTICLE INFO

Keywords:
Agricultural biomass burning
Secondary BrC
MRS and percentile methods
Weather conditions

ABSTRACT

Measurements of absorption optical properties ($\sigma_{ap,\lambda}$, AAE) and PM_{10} concentrations were conducted near the rice fields of L'Albufera Natural Park (Eastern Spain) with the aim of assessing light absorption by secondary BrC generated from the burning of rice straw residues. Sampling was performed in autumn 2023. The measurement period was divided into three sub-periods (P_1, P_2 and P_3) depending on the number of burning spots and the prevailing weather conditions. P_2 was the period most affected by biomass burning (BB) events. During this period, hourly values of $\sigma_{ap,\lambda}$ and AAE were above 100 Mm^{-1} and 2.0 and BrC absorption was higher than BC absorption in the UV spectral range. Secondary BrC concentrations were estimated using the EC-tracer method, and the R-squared (MRS) and 25 % percentile (P25) approaches were applied to the determination of $(\sigma_{ap,\lambda}/BC_{880})_{pri}$. Secondary BrC concentrations calculated by the P25 method were significantly higher than those obtained by the MRS approach for P_2, which lead to $\sigma_{BrC\text{-}SEC}$ values four times higher when the P25 method was used. The differences in the results obtained by both procedures were attributed to the formation of secondary BrC generated from the rapid oxidation of semi-volatile organic aerosols emitted by BB. The contribution of this secondary BrC to light absorption by BrC at 370 nm was 47 % for P_2.

1. Introduction

Biomass burning (BB) has been recognized as a major source of aerosols due to the emission of gaseous precursors and particulate pollutants into the atmosphere (Koppmann et al., 2005). As a consequence, BB has significant impacts on regional and local air quality (Chen et al., 2017), as well as on public health (Sigsgaard et al., 2015; Van Den Heuvel et al., 2018). On the other hand, the combustion of wood and crop residues in rural areas emits large quantities of light-absorbing carbonaceous aerosols, such as black carbon (BC) and brown carbon (BrC; i.e., light-absorbing organic carbon) (Chakrabarty et al., 2010), thereby affecting the Earth's radiation budget (Bond et al., 2013). In fact, the most important primary source of BrC is BB (Washenfelder et al., 2015; Zhang et al., 2020). BrC can also be formed via oxidation of volatile organic compounds or transformation of primary BrC during ageing processes in the atmosphere, and hence may be secondary in nature (Gilardoni et al., 2016; Laskin et al., 2015). The global contribution of BrC to radiative forcing is +0.25 W m^{-2} or 19 % of the absorption by anthropogenic aerosols (Feng et al., 2013). For aged aerosols, when the absorptivity is analysed in terms of MAE (Mass Absorption Efficiency), secondary organic aerosols (SOA) typically show low absorptivity values. Nevertheless, previous studies have reported that secondary BrC can be more absorptive at short visible wavelengths than primary BrC (Saleh et al., 2013). Therefore, secondary BrC may be an important contributor to the global radiative forcing budget.

Different approaches have been used in order to determine the absorption coefficient of secondary BrC ($\sigma_{BrC\text{-}SEC}$). The elemental carbon (EC) tracer method (Turpin and Huntzicker, 1995) can be used as an initial approach for calculating $\sigma_{BrC\text{-}SEC}$. This method requires the determination of the ratio of the primary particle's absorption to the BC mass concentration from combustion sources. Different methodologies can be used to quantify $\sigma_{BrC\text{-}SEC}$ depending on the way to estimate this ratio. Two of the most common techniques are the Minimum-R squared (MRS) method (Wang et al., 2019), and the use of the lower percentiles of the OC/EC data (Kaskaoutis et al., 2020; Sheoran et al., 2021). The first approach produces robust results, but it may significantly

* Corresponding authors.
E-mail addresses: j.nicolas@umh.es (J.F. Nicolás), amalia@ceam.es (A. Muñoz).

https://doi.org/10.1016/j.atmosres.2025.108239
Received 5 March 2025; Received in revised form 12 May 2025; Accepted 24 May 2025
Available online 29 May 2025

underestimate SOC (or secondary BrC) levels in environments highly affected by BB emissions (Kaskaoutis et al., 2020), whereas the second leads to an overestimation of $\sigma_{BrC,\lambda\text{-SEC}}$ because a significant fraction of the SOC obtained by this method corresponds to primary BB emissions (Kaskaoutis et al., 2020).

The main objective of this study is to quantify light absorption by secondary BrC from BB emissions. For that purpose, the sampling site was located near the rice fields of L'Albufera Natural Park (eastern Spain), where massive burning of rice straw occurs in early autumn each year. A comparative estimation of secondary BrC levels by the EC-tracer method using the two approaches previously mentioned was also performed.

2. Experimental

2.1. Sampling site

The study area (L'Albufera Natural Park-ANP) is situated in the region of Valencia (eastern Spain) and extends over an area of approximately 21,000 ha. The ANP is one of the most important wetlands in Southern Europe (Torregrosa et al., 2021). This area contains a coastal pine forest and a lagoon surrounded by rice fields, which are the main agricultural crop with a production of 116,925 t and a surface of 15,087 ha (Food and Agriculture Organization of the United Nations, 2018). The ANP is surrounded by several urban areas. The delimitations between the rice crop areas and the urban locations can be seen in Torregrosa et al. (2021).

The ANP has a mild Mediterranean climate, with an annual average humidity of 65 % and an average temperature of 18 °C. Precipitation usually occurs in autumn, with an average annual value of 450 mm, although during the study period no precipitation was recorded. The valley is dominated by sea-breeze circulations during warm periods (Pérez-Landa et al., 2007).

The monitoring site (−0.319 W, 39.315 N) was located inside the ANP, to the south of the lake (Fig. 1), approximately 10 km from the city of Valencia.

In 1990, the ANP was designated as a Ramsar Site in the list of wetlands of international importance for birds and it is considered a Special Protection Area since 1991.

2.2. Characterization of rice straw burning

The controlled burning of rice straw is carried out through the monitoring program QUEPAR (https://www.ceam.es/ceamet/QUEPAR/web/APP_QUEPAR.htm) that forecasts the favourable/unfavourable dispersive conditions 24 h before the start of agricultural residue burning, minimizing the potential impact on major population centres. Favourable dispersion conditions occur when the wind blows towards the sea. This situation is associated with the predominance of local or regional winds, such as sea breezes. On the other hand, a requirement that must be addressed is that no thermal inversion is detected. By means of a mobile phone application, farmers must register at the moment of starting straw burning, always under appropriate environmental conditions, leaving a record of the time and plot (coordinates and extension) burned.

The burning period was from 06/10/2023 to 23/11/2023. During this period, biomass burning occurred on 32 days. Fig. 2 shows the number of burning episodes (N) and the surface burned.

A total of 709 burning episodes were identified, most of them between 16 and 20 October (~75 %). During this period, more than 3600 t of rice straw were burned. A high number of burning events also occurred between 23 and 30 October (although they were noticeably lower). Less than 10 episodes per day were occasionally identified the remaining days.

Burning episodes usually started early in the morning (08:00–10:00 h) and continued until early afternoon. However, the days with the highest number of burning episodes ($N > 50$), fires continued until

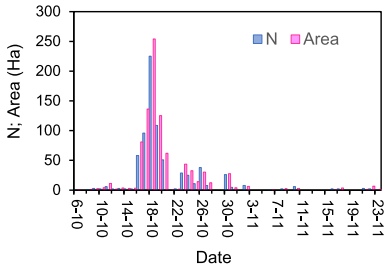

Fig. 2. Number of burning spots and surface burned each day of the study period.

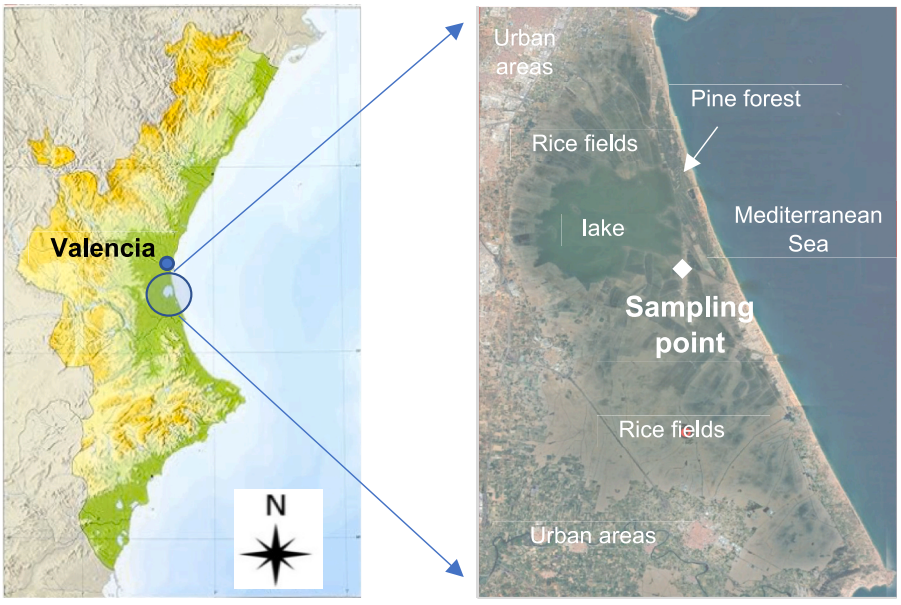

Fig. 1. Location of the sampling site, the rice fields and the nearby urban areas.

21:00–22:00 h. As an example, Fig. S1 (supplementary material) shows the location of the fire spots for the day with the highest number of burning events (18/10/23). In general, the highest number of burning events occurred to the south-west of the sampling site.

On days with a low number of burning events, the detection of burning emissions at the sampling site depended on the meteorological conditions (mainly wind speed and direction) and the distance to the fires. However, on days with a large number of burning spots around the sampling site (for instance 18/10/23, Fig. S1), biomass burning emissions had a significant impact at the measurement site.

2.3. Measurement of light absorption properties

To determine the light absorption by atmospheric aerosols ($\sigma_{ap,\lambda}$), an Aethalometer model AE33 (Magee Scientific, USA) was used. Initially, the AE33 provides light attenuation values of the particulate matter accumulated on a mobile filter at seven different wavelengths ranging from UV to IR: 370, 470, 520, 590, 660, 880, and 950 nm. However, the obtained attenuation value is higher than the actual absorption due to the multiple scattering effect of filter fibres and increased particle loading on the filter. To correct this effect, a factor depending on the filter type was used, which in this case was 1.76 (Savadkoohi et al., 2023). Absorption measurements were performed for approximately one month in 2023, from the beginning of the burning season until early November. The instrument operated at a constant airflow rate of 5 $l{\cdot}min^{-1}$. The temporal resolution was 1 min. Hourly and daily averages of σ_{ap} were calculated from these data.

The Absorption Angstrom Exponent (AAE) was obtained using a log-linear regression approach (Schuster et al., 2006).

To calculate the contributions of biomass burning (BC_{BB}) and fossil fuel combustion (BC_{FF}) to BC emissions, the method developed by Sandradewi et al. (2008) was used.

The procedures applied to estimate the different contributions to $\sigma_{ap,\lambda}$: absorption by BC ($\sigma_{BC,\lambda}$), BrC ($\sigma_{BrC,\lambda}$) and secondary BrC ($\sigma_{BrC,\lambda\text{-SEC}}$) are described in the next section.

2.4. Estimation of the contributions to $\sigma_{ap,\lambda}$

In order to calculate the different contributions to σ_{ap}, it has to be assumed that BrC and BC are the only absorbing aerosols. However, during the measurement period, a Saharan dust event (SDE) occurred between 14/10/23 and 18/10/23. This event, which had a limited impact at the study area based on the mineral dust load, is illustrated in the supplementary material (Fig. S2). Therefore, the total absorbed radiation was corrected by subtracting the contribution due to mineral dust ($\sigma_{Dust,\lambda}$) during this event.

2.4.1. Determination of $\sigma_{Dust,\lambda}$

Considering that the total absorption coefficient ($\sigma_{ap,\lambda}$) is divided into 3 components: $\sigma_{BC,\lambda}$, $\sigma_{BrC,\lambda}$ and $\sigma_{Dust,\lambda}$ (Eq. (1)):

$$\sigma_{ap,\lambda} = \sigma_{BC,\lambda} + \sigma_{BrC,\lambda} + \sigma_{Dust,\lambda} \quad (1)$$

the approximate contribution of mineral dust to light absorption can be obtained from $MAE_{Dust,\lambda}$ values and mineral dust concentration according to Eq. (2):

$$\sigma_{Dust,\lambda} = [C_{Dust}] \times MAE_{Dust,\lambda} \quad (2)$$

$MAE_{Dust,\lambda}$ values were calculated using the data from Caponi et al. (2017) for $PM_{10.6}$. The values obtained were: 0.097, 0.063, 0.042, 0.031 and 0.023 $m^2{\cdot}g^{-1}$ at 370, 470, 520, 590 and 660 nm, respectively. Dust concentrations [C_{Dust}] were estimated using the equation proposed by Guinot et al. (2007) (Eq. (3)), since no data on Al and Si concentrations were available in this study:

$$[C_{Dust}] = [nss - Ca^{+2}]/f \quad (3)$$

where [nss-Ca^{+2}] is the non-sea salt soluble calcium and the coefficient f represents the abundance of soluble calcium in mineral dust. In the present work, the factor of 0.11 determined by Galindo et al. (2020) for intrusion days was applied. Total calcium concentrations measured by ED-XRF were used, which provide an upper limit for mineral dust absorption. The daily σ_{Dust} during intrusion days did not exceed 6 % of the σ_{ap} at 370 nm, indicating a limited influence of mineral dust on the absorption process. The values of $\sigma_{Dust,\lambda}$ (Table S1 of the supplementary material) were subtracted from the total absorption coefficient during this period.

2.4.2. Determination of $\sigma_{BC,\lambda}$ and $\sigma_{BrC,\lambda}$

Once the mineral dust absorption was removed, the absorption coefficient can be written as:

$$\sigma_{ap,\lambda} = \sigma_{BC,\lambda} + \sigma_{BrC,\lambda} \quad (4)$$

The methodology described by Kaskaoutis et al. (2021), called the *BrC model*, was used to determine the contribution from BrC to light absorption. This approach assumes that BC is the only absorbing component at 880 nm and that its spectral dependence for the other wavelengths follows a λ^{-1} function. The contribution of BrC for each wavelength was subsequently estimated using Eq. (4) from the differences between $\sigma_{ap,\lambda}$ and $\sigma_{BC,\lambda}$ values. This procedure has been widely used to determine the value of $\sigma_{BrC,\lambda}$ from Aethalometer measurements (Nicolás et al., 2018; Gilardoni et al., 2020; Pani et al., 2021). The uncertainty in the estimated absorption coefficients of BC and BrC using this methodology is 25 % (Park et al., 2018).

2.4.3. Procedures to quantify $\sigma_{BrC,\lambda\text{-}SEC}$

Two different procedures were used to calculate $\sigma_{BrC,\lambda\text{-SEC}}$. Both are commonly used to determine the mass concentration of secondary organic carbon (SOC) and are based on the EC tracer approach, which requires a prior estimation of the ratio of primary OC to EC $(OC/EC)_{pri}$. The two methods differ in the determination of this ratio. When applied to the estimation of the light absorption by SOC, the equivalent ratio to be obtained is $(\sigma_{ap,\lambda}/BC_{880})_{pri}$, which is the ratio of the primary particle's light absorption to the BC mass concentration from combustion sources.

a) Minimum-R squared (MRS) method: The absorption by BrC is calculated using Eq. (5) (BC tracer approach) assuming a negligible effect of primary biogenic BrC.

$$\sigma_{BrC,\lambda-SEC} = \sigma_{ap,\lambda} - \left(\sigma_{ap,\lambda}/BC_{880}\right)_{pri} \times [BC_{880}] \quad (5)$$

The determination of $(\sigma_{ap,\lambda}/BC_{880})_{pri}$ using the MRS method is described in detail in Wang et al. (2019). This method is based on the assumption that SOC is inherently unrelated to EC and thus the estimated absorption by BrC_{SEC} must not be correlated with BC_{880} ($R^2 \sim 0$) (Kaskaoutis et al., 2021). Briefly, arbitrary values for $(\sigma_{ap,\lambda}/BC_{880})_{pri}$ from 0 up to a maximum value of 60 with an increment of 0.1 were employed, and a series of coefficients of determination (R^2) were then calculated. The optimal ratio was defined as that which provided the minimum R^2 value, indicating that BrC was not from primary sources but from ageing processes.

This methodology has been widely used in the literature (Wang et al., 2019; Liakakou et al., 2020; Zhu et al., 2021; Gao et al., 2022; Xu et al., 2024). However, as previously mentioned, $\sigma_{BrC,\lambda\text{-SEC}}$ obtained by this procedure is underestimated, especially in environments highly impacted by BB aerosols (Kaskaoutis et al., 2021). The reason is that this method considers the fraction of $\sigma_{BrC,\lambda\text{-SEC}}$ that is not correlated with BC, but not the fraction of BrC absorption due to secondary organic aerosols formed from the rapid oxidation of precursors co-emitted with BC during biomass combustion (Wu et al., 2019). The bias of the MRS results is generally below 23 % when the measurement uncertainty is within 20 % (Wu and Yu, 2016).

b) The Percentile method: This method is based on the use of the lower percentiles (5–25 %) of the $\sigma_{ap,\lambda}$/BC data to calculate the ($\sigma_{ap,\lambda}$/

$BC_{880})_{pri}$ ratio. In the present work, the 25th percentile was used and $\sigma_{BrC,\lambda\text{-SEC}}$ was subsequently estimated from Eq. (8). In environments impacted by BB, the $(OC/EC)_{pri}$ is mostly related to vehicular emissions. Therefore, $\sigma_{BrC,\lambda\text{-SEC}}$ obtained by the percentile method would correspond to an amount with a significant influence from primary BB emissions, leading to an overestimation of $\sigma_{BrC,\lambda\text{-SEC}}$ (Kaskaoutis et al., 2020).

The difference between $\sigma_{BrC,\lambda\text{-SEC}}$ estimated by both methods can be attributed to light absorption by secondary organic aerosols generated from the rapid oxidation of precursors emitted from both fossil fuel combustion and BB (Wu et al., 2019; Kaskaoutis et al., 2020). Therefore, this difference could be used to estimate the absorption by secondary BrC related to emissions produced during biomass combustion.

In this study, the primary ratios were estimated separately for daytime (08:00 h–20:00 h) and night-time (21:00 h–07:00 h).

2.5. PM_{10} sampling and analysis

PM_{10} daily sampling was carried out between 6 October and 1 November by means of an MCV high volume sampler (30 $m^3 \cdot h^{-1}$). A total of 27 samples were collected onto 150-mm quartz fibre filters (MK 360, Ahlstrom) during the measurement campaign. Mass concentrations were determined gravimetrically using a Mettler-Toledo model XP105 analytical balance with 10 μg sensitivity. Filters were kept in controlled conditions (20 ± 1 °C and 50 ± 5 % relative humidity) for at least 24-h and weighted in quadruplicate before and after sampling. Filters were stored in the fridge at 4 °C until chemical analyses.

Although the study of PM_{10} chemical composition during biomass burning episodes is not an objective of this work, some PM_{10} components were analysed because they are tracers of biomass burning emissions (e.g. levoglucosan) and Saharan dust outbreaks (e.g. titanium, Galindo et al., 2018) (Fig. S2). On the other hand, calcium concentrations were used to estimate the concentration of mineral dust as described in Section 2.4.1. Therefore, PM_{10} samples were analysed by energy dispersive X-ray fluorescence (ED-XRF) for major and trace elements, and by high performance anion exchange chromatography with pulsed amperometric detection (HPAEC-PAD) to determine the levoglucosan content. In the elemental analysis, minimum detection limits (MDLs) were determined as described in Giannoni et al., 2015. For levoglucosan, MDLs were calculated as 2σ.

The elemental composition of PM_{10} samples was determined by means of an ARL Quant'x Spectrometer (Thermo Fisher Scientific, UK) with a Si(Li) detector. A detailed description of the analytical technique can be found elsewhere (Chiari et al., 2018).

The analysis of levoglucosan was performed by means of a Thermo Scientific Dionex Integrion system equipped with an electrochemical detector and a Dionex Carbopac PA10 analytical column (250 × 4 mm). NaOH was used as a carrier solvent at a flow rate of 0.5 ml min^{-1}. The gradient was: 18 mM (0–2 min), 200 mM (2–9 min; column cleaning), 18 mM (9–29 min; equilibration). For the amperometric detection a gold working electrode was used.

Summary statistics of PM10 components, are presented in Table S2 (supplementary material).

3. Results and discussions

3.1. Impact of rice straw burning on optical absorption properties (OAP)

The hourly and daily evolution of $\sigma_{ap,370}$ and AAE from the beginning of the biomass burning period until 27 October is shown in Fig. 3. The study of aerosol optical properties was extended until 27 October. After that date, burning episodes were sporadic.

At the beginning of the measurement period, daily values of $\sigma_{ap,370}$ oscillated between 10 and 20 Mm^{-1}, while AAE values were below 1.3. During these days, occasional burning of rice straw in the fields surrounding the sampling site occurred. AAE and $\sigma_{ap,370}$ values increased

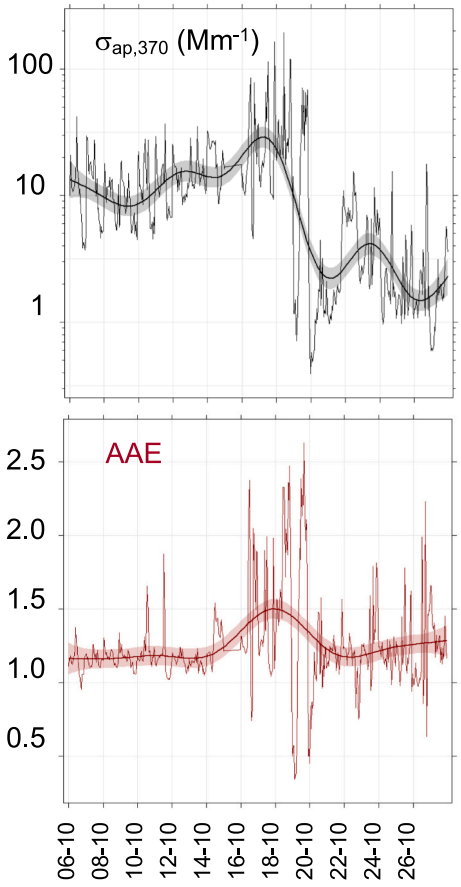

Fig. 3. Daily and hourly evolution of $\sigma_{ap,\lambda}$ and AAE during the study period.

significantly between 16 and 19 October due to the occurrence of intense burning events. Values higher than 2.0 for AAE and 100 Mm^{-1} for $\sigma_{ap,370}$ were observed. From 20 October onwards the absorption coefficient decreased, despite there were some burning events. Although AAE values also decreased, they were slightly higher than those recorded on the first days of the measurement period, suggesting a greater contribution from the BB source. This high variability can be attributed to changes in meteorological conditions. During the first ten days of the study period the dominant weather pattern corresponded to an anticyclonic situation, characterized by atmospheric stability and local winds. From 20 October strong winds coming from the Atlantic (west direction, 270°) induced a sweeping effect, resulting in a significant decrease in PM levels (Fig. S2, supplementary material) and $\sigma_{ap,\lambda}$. The remarkable reduction in PM_{10} concentrations was also observed between 23 and 27 October, when some burning events occurred, as already mentioned. The synoptic meteorological conditions for a day at the beginning and end of the measurement period are shown in Fig. S3 (supplementary material). The days with the highest number of burning events, meteorological conditions may be considered as transitional between the two periods.

Based on the differences between the predominant weather patterns and the number and intensity of burning events, the measurement period was divided into three sub-periods (P_i, Table 1). As clearly seen, OAP values were affected by the number of burning episodes and the prevailing meteorological conditions.

The highest values of OAP were registered during P_2 due to the high number of burning events. During this period, the average solar radiation was lowest, most likely due to the smoke generated during rice straw burning. An increase of almost 15 $\mu g \cdot m^{-3}$ in PM_{10} concentrations was observed between P_1 and P_2, similarly to the study by Viana et al. (2008). Although the number of burning episodes was significantly

Table 1
Mean values of OAP, meteorological parameters, number of burning events and PM_{10} concentrations during the three sub-periods.

	P_1	P_2	P_3
Date	06/10–15/10	16/10–19/10	20/10–27/10
N	<3	123	21
V_{wind} ($m \cdot s^{-1}$)	2.9	4.1	6.0
T (°C)	21.3	22.1	19.0
RH (%)	86.6	75.5	65.9
SR ($W \cdot m^{-2}$)	152.0	100.8	115.2
$\sigma_{ap,370}$ (Mm^{-1})	13.1	34.0	3.2
$AAE_{370-950}$	1.22	1.78	1.27
%BB	16.5	38.4	21.4
PM_{10} ($\mu g \cdot m^{-3}$)	24.3	38.2	6.3

N: average daily burnings for each period.

higher during P_3 than during P_1, the absorption coefficient was much lower due to the high wind speeds during this period (Fig. S3).

3.2. $\sigma_{BC,\lambda}$ and $\sigma_{BrC,\lambda}$

3.2.1. Contribution of BrC to light absorption

The absorption coefficients of BC and BrC for the whole measurement period and for each sub-period are presented in Table 2.

The average contribution of BrC to total absorption at 370 nm was 37.3 % and decreased to 3.6 % at 660 nm. During P_1 and P_3, the percentage contributions at 370 nm were 17.6 % and 24.0 %, respectively. Unsurprisingly, during the period with the highest number of burning events the contribution of BrC to light absorption increased above 56 %. This value was slightly lower than that found in northern China (63 %, $\lambda = 375$ nm) during rice straw burning (Wang et al., 2020). During P_2, the absorption by BrC was closely related to rice straw burning, as can be seen in Fig. 4. This figure shows the relationship between $\sigma_{BrC,370}$ and daily concentrations of levoglucosan, used as a tracer for BB.

The data corresponding to each sub-period can be clearly differentiated and demonstrate the relationship between absorption by BrC and levoglucosan levels.

Table 3 shows AAE values for BrC absorption averaged for the three sub-periods and the whole study period.

In general, AAEBrC values during BB events were higher than those recorded for ambient aerosols (Shen et al., 2017), since BB chromophores effectively absorb radiation in the shorter wavelength range. For this reason, the average AAE value (5.38) was higher than that obtained in the city of Elche (4.80), which is relatively close to the sampling site (López-Caravaca et al., 2024; Rovira et al., 2025). The highest AAEBrC value was obtained during the second period, most likely because P2 is the period that best characterized the BB environment. The average AAE value was slightly higher than that found in China (5.0 ± 0.1) during rice straw burning (Wang et al., 2020) and similar to that obtained during winter (5.5 ± 1.1) in the city of Ioannina (Grecce) under intense residential wood burning conditions (Paraskevopoulou et al., 2023).

Table 2
Mean values of $\sigma_{BC,\lambda}$ and $\sigma_{BrC,\lambda}$ (Mm^{-1}) for the overall study period and the three sub-periods.

	Global		P_1		P_2		P_3	
λ (nm)	σ_{BC}	σ_{BrC}	σ_{BC}	σ_{BrC}	σ_{BC}	σ_{BrC}	σ_{BC}	σ_{BrC}
370	8.26	4.76	10.76	2.30	13.68	17.54	2.43	0.76
440	6.95	2.11	9.05	1.56	11.50	6.26	2.05	0.33
520	5.88	1.21	7.66	0.95	9.73	3.03	1.73	0.16
590	5.61	0.59	6.75	0.45	8.57	1.28	1.53	0.06
660	4.63	0.17	6.03	0.15	7.67	0.62	1.36	0.03
880	3.47		4.52		5.75		1.02	
950	3.22		4.20		5.32		0.95	

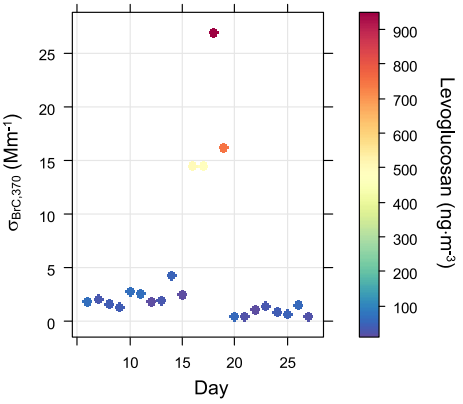

Fig. 4. Daily variation of the contribution of BrC to light absorption at 370 nm as a function of levoglucosan concentration ($ng \cdot m^{-3}$).

Table 3
AAE values computed by a power-law fit of the absorption coefficients of BrC.

	$AAE_{BrC\ (370-660\ nm)}$
Global	5.38 ± 0.72
P_1	4.46 ± 0.79
P_2	5.68 ± 0.24
P_3	5.20 ± 0.35

3.3. Characterization of secondary BrC

Secondary BrC levels were estimated using the two methods described in Section 2.4.3 (MRS and P25). Since the relative contributions of primary emission sources may vary depending on the period analysed, a different $(\sigma_{ap,\lambda}/BC_{880})_{prim}$ ratio was determined for each sub-period (for both day and night).

The ratios (day-night) calculated using the MRS approach at 370 nm for each sub-period were: P_1 (14.2–12.4 $m^2 \cdot g^{-1}$), P_2 (33.8–26.8 $m^2 \cdot g^{-1}$) and P_3 (13.6–13.8 $m^2 \cdot g^{-1}$). An Igor-based program was used for the calculation of these ratios (Wu et al., 2018; Wu et al., 2023; Wu and Yu, 2016). As an example, Fig. S4 shows how this ratio was calculated for night-time for P_1. On the other hand, the values obtained at 370 nm using the P25 method, were: P_1 (12.0–12.2 $m^2 \cdot g^{-1}$), P_2 (18.9–12.3 $m^2 \cdot g^{-1}$) and P_3 (11.7–11.3 $m^2 \cdot g^{-1}$). The values of $\sigma_{BrC,\lambda\text{-SEC}}$ were subsequently estimated from both methods.

3.3.1. Hourly variation of secondary BrC

Daily patterns of $\sigma_{BrC,\lambda\text{-SEC}}$ calculated by the P25 method ($\sigma_{BrC,\lambda\text{-SEC-P25}}$) at 370 nm during the three sub-periods are shown in Fig. 5.

During P_1, less influenced by BB emissions than the other two periods (Table 1), the hourly absorption showed a peak around noon (10:00–14:00 h). The increase in solar radiation after sunrise promotes photochemical reactions that led to the formations of secondary BrC. The decrease in $\sigma_{BrC,\lambda\text{-SEC}}$ from 15:00 h can be explained considering that light absorbing chromophores were bleached through oxidative processes (Wang et al., 2019).

In the second period (the most affected by BB emissions), the average absorption by secondary aerosols was very high during the day because burning episodes occurred during the morning and afternoon hours. The peak observed around midday was higher than in P_1 because the BrC produced after the fast oxidation of BB precursors increased the total secondary BrC. The values of the absorption coefficient were high from early afternoon until evening (15:00–21:00 h) due to emissions during burning events (Fig. S1).

The values of $\sigma_{BrC,\lambda\text{-SEC}}$ during P_3 were influenced by the synoptic situation. Strong winds resulted in a reduction of PM_{10} levels (lower

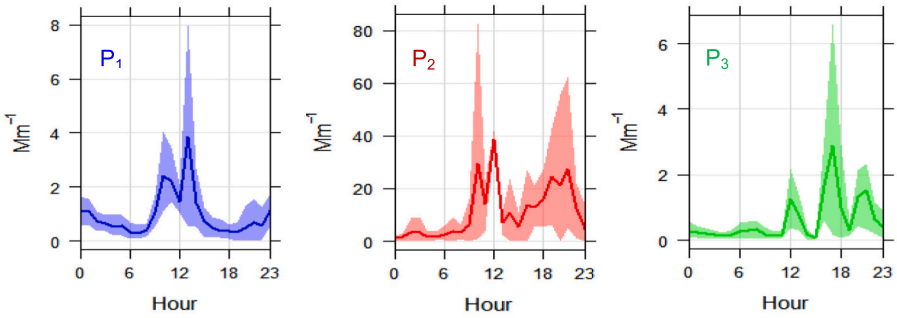

Fig. 5. Hourly variation of $\sigma_{BrC\text{-}SEC}$ at 370 nm during the three sub-periods (P_1-blue, P_2-red and P_3-green). (For interpretation of the references to colour in this figure legend, the reader is referred to the web version of this article.)

than 7.0 μg·m^{-3}), thus affecting also BrC absorption (Table 2). The variability of $\sigma_{BrC,\lambda\text{-}SEC}$ showed small maxima during the afternoon, maybe due to sporadic burning events.

3.3.2. *Comparison of procedures for the quantification of $\sigma_{BrC,\lambda\text{-}SEC}$*

Fig. 6a shows average values of $\sigma_{BrC,\lambda\text{-}SEC}$ at 370 nm determined by both methods. For P_1 and P_3 the absorption coefficients calculated using the P25 method were slightly higher than those obtained by the MRS approach. In contrast, the difference between the values calculated by both methods were considerably higher for P_2. This was due to the high number of burning events during this period, leading to an overestimation of secondary BrC absorption by the P25 method and an underestimation of secondary BrC absorption by the MRS approach. Similar results were obtained in Ioannina (Greece), a city highly impacted by wood combustion (Kaskaoutis et al., 2020). The average absorption coefficient of secondary BrC obtained by the P25 method

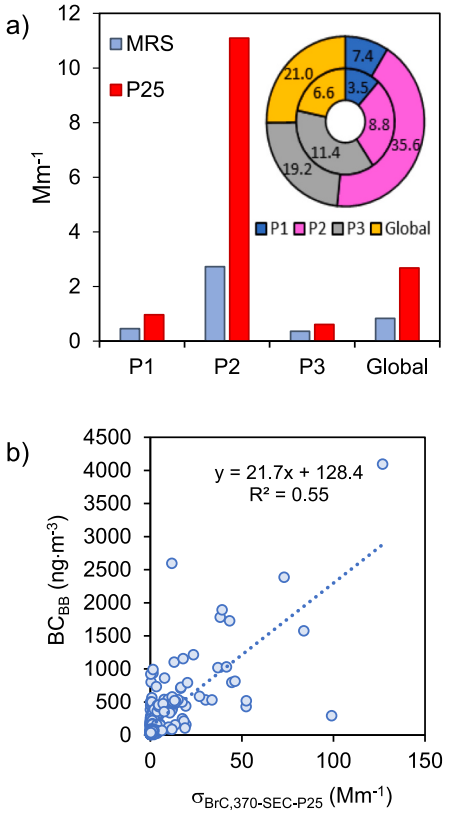

Fig. 6. a) Values of $\sigma_{BrC\text{-}SEC}$ for the three sub-periods calculated using the 25th percentile and MRS methods; b) correlation between the secondary BrC absorption derived via 25 % percentile and BC_{BB}.

($\sigma_{BrC,\lambda\text{-}SEC\text{-}MRS}$ = 2.68 Mm^{-1}) was almost three times higher than that calculated using the MRS approach ($\sigma_{BrC,\lambda\text{-}SEC\text{-}P25}$ = 0.84 Mm^{-1}).

On a percentage basis, the contribution of secondary BrC to total absorption calculated by the MRS method was 6.6 %, while this percentage increased to 21 % when it was calculated by the P25 method, as shown in Fig. 6a. The influence from primary BB emissions on $\sigma_{BrC,\lambda\text{-}SEC\text{-}P25}$ was demonstrated by the correlation with BC_{BB} (Fig. 6b). No correlation between $\sigma_{BrC,\lambda\text{-}SEC\text{-}P25}$ and BC_{FF} was found (R^2 = 0.06).

As already indicated, the difference between $\sigma_{BrC,\lambda\text{-}SEC}$ calculated by both methods can be attributed to the contribution of secondary BrC generated form the rapid oxidation of BB precursors (Wu et al., 2019; Kaskaoutis et al., 2020). The average differences between $\sigma_{BrC,\lambda\text{-}SEC\text{-}P25}$ and $\sigma_{BrC,\lambda\text{-}SEC\text{-}MRS}$ were 1.88, 0.51, 8.56 and 0.24 Mm^{-1} for the whole study period, P_1, P_2 and P_3, respectively. As expected, the highest difference was obtained for P_2, when almost 78 % of $\sigma_{BrC,\lambda\text{-}SEC}$ was due to secondary BrC formed from the oxidation of precursors emitted during rice straw burning. The correlation between levoglucosan and the difference in $\sigma_{BrC,\lambda\text{-}SEC}$ estimated by the two procedures is showed in Fig. S5. The high correlation coefficient supports the role of BB emissions on the magnitude of this difference. Nevertheless, it has to be considered that average daily values were used for the correlation analysis and, therefore, the result of the correlation was highly influenced by the data included in P_2.

3.4. *Contribution of different aerosols to light absorption*

Absorption by primary BrC ($\sigma_{BrC\text{-}PRI}$) was calculated by subtracting the value of $\sigma_{BrC\text{-}SEC\text{-}P25}$ to that of σ_{BrC}. This may lead to an underestimation of $\sigma_{BrC\text{-}PRI}$ calculated by the P25 method, since $\sigma_{BrC,\lambda\text{-}SEC}$ obtained by this procedure was overestimated, as already mentioned. This is especially evident for P_3, when BrC absorption was lower than 0.2 Mm^{-1} at $\lambda > 520$ nm (Table 2). Considering the errors in the determination of each component, it is worth indicating that the results for P_3 at $\lambda > 520$ nm may not be reliable. It has to be mentioned that, in this section, $\sigma_{BrC\text{-}SEC\text{-}MRS}$ was named as $\sigma_{BrC\text{-}SEC1}$. The value of $\sigma_{BrC\text{-}SEC1}$ represents the absorption by secondary BrC not generated from the oxidation of precursors emitted during rice straw burning. The origin of this BrC is associated with the value of $\sigma_{BrC\text{-}SEC2}$, which has been calculated through the difference between $\sigma_{BrC,\lambda\text{-}SEC\text{-}P25}$ and $\sigma_{BrC,\lambda\text{-}SEC\text{-}MRS}$.

Fig. 7 shows the average absorption by BC, BrC_{PRI}, BrC_{SEC1} and BrC_{SEC2} as a function of the wavelength, as well as the percentage contribution of each component to total light absorption. The daily variability of the contribution of each component to total light absorption at 370 nm is shown in Fig. S6.

The average contribution of $\sigma_{BrC\text{-}SEC2}$ to the total light absorption by BrC at 370 nm was 47 % for P_2. This contribution was significantly higher than that calculated for P_1 and P_3, pointing to the critical role of BB emission on the formation of secondary BrC (Wu et al., 2023). The percentage contribution at other wavelengths was around 40 % for P_2. The contribution of $\sigma_{BrC\text{-}SEC2}$ to σ_{BrC} was three times higher than that of

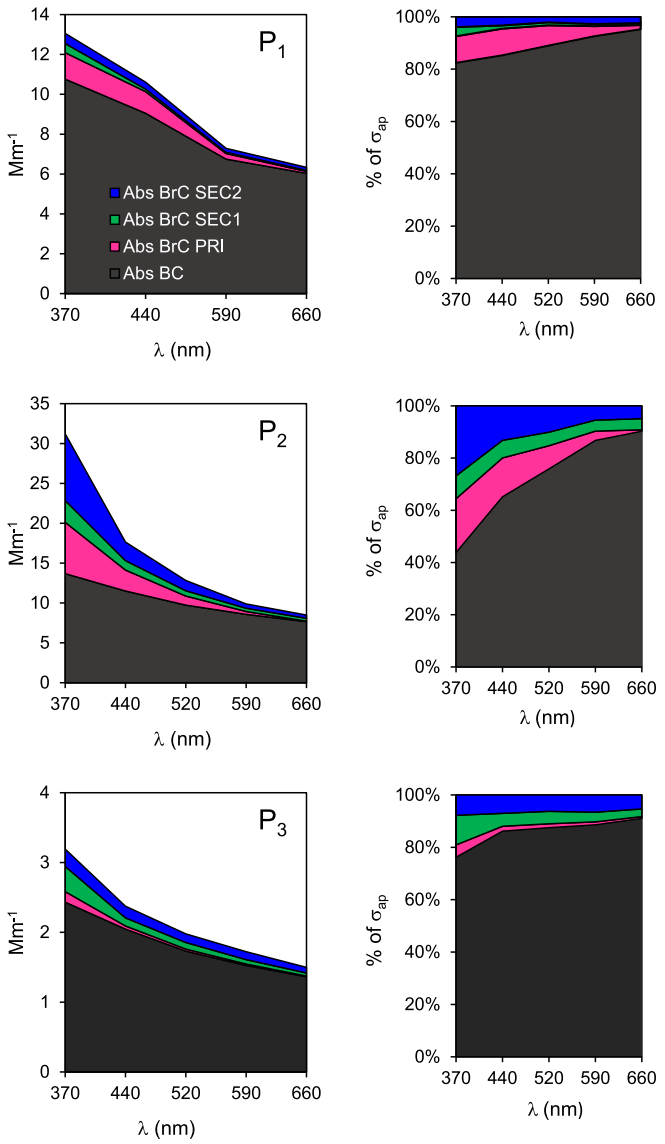

Fig. 7. Average absorption coefficients of BC, BrC_{PRI}, BrC_{SEC1} and BrC_{SEC2} as a function of the wavelength for P_1, P_2 and P_3. The contribution (%) of each aerosol component to the mean absorption is also shown.

$\sigma_{BrC\text{-}SEC1}$ at 370 nm. However, in the visible region the contributions of $\sigma_{BrC\text{-}SEC2}$ and $\sigma_{BrC\text{-}SEC1}$ to σ_{BrC} were comparable. In contrast, for P_1 and P_3 the contributions of $\sigma_{BrC\text{-}SEC2}$ to σ_{BrC} at 370 nm were similar.

4. Conclusions

The impact of open burning of rice residues on PM_{10} levels and aerosol optical absorption properties has been evaluated during a field campaign in L'Albufera Natural Park (eastern Spain). The following conclusions were extracted from this study:

- During the period with the highest number of burning episodes (P_2), BrC absorption in the UV spectral range was higher than the absorption by BC. During this period, the absorption by secondary BrC formed from the rapid oxidation of semi-volatile organic aerosols emitted by BB accounted for almost half of the total BrC light absorption at 370 nm.
- In BB-impacted environments, the values of $\sigma_{BrC\text{-}SEC}$ were highly dependent on the method used to determine $(\sigma_{ap,\lambda}/BC_{880})_{pri}$, with differences up to almost 30 %.
- The prevailing meteorological conditions in the study area can have a significant influence on PM concentrations and $\sigma_{ap,\lambda}$ values, independently of the number of burning episodes. Strong winds may result in a sweeping effect, leading to significant decreases in PM levels and absorption values. This was observed at the end of the measurement period (P_3), when $\sigma_{ap,\lambda}$ values and PM_{10} concentrations were four times lower than those at the beginning of the campaign (P_1), although a higher number of burning episodes were identified during P_3.

The open-field burning of rice straw in L'Albufera Natural Park poses a significant potential environmental risk, particularly to air quality. This practice emits considerable amounts of pollutants at ground level, especially particulate matter, in a region close to densely populated areas. To reduce its impact on the atmospheric environment, the burning of part of the straw is a controlled activity only permitted under favourable dispersive conditions (i.e., when the wind blows towards the sea). This seems to be the best option compared to others alternatives, such as on-site straw burning for use in other sectors or controlled straw burning for electricity generation. However, the meteorological conditions under which controlled burns occur (predominance of sea breezes) can favour the production of secondary pollutants, especially of a photochemical nature, since the species emitted the day before return inland during the subsequent period of onshore flow and interact with fresh emissions. Future research is needed to evaluate this effect.

CRediT authorship contribution statement

B. Domínguez: Writing – original draft, Investigation, Conceptualization. **J.F. Nicolás:** Conceptualization, Writing – original draft, Investigation. **E. Mantilla:** Data curation. **C. Gimeno:** Data curation. **E. Borrás:** Data curation. **M. Ródenas:** Resources, Data curation. **T. Vera:** Resources, Funding acquisition, Data curation. **R. Soler:** Resources, Data curation. **M. Alfosea-Simón:** Formal analysis, Data curation. **E. Yubero:** Formal analysis. **J. Crespo:** Supervision, Funding acquisition. **N. Galindo:** Writing – review & editing, Supervision, Funding acquisition. **A. Clemente:** Data curation. **A. Muñoz:** Writing – review & editing, Supervision, Funding acquisition.

Declaration of competing interest

The authors declare that they have no known competing financial interests or personal relationships that could have appeared to influence the work reported in this paper.

Acknowledgements

This work was supported by the ATMOBE R+D project (PID2022-142366OB-I00), funded by MCIN/AEI/10.13039/501100011033/, the "ERDF A way of making Europe", and the EVER project (CIPROM/2022/37) funded by GVA. The research was also funded through the CAMBIO project (TED2021-131336B-I00) granted by MCIN/AEI/10.13039/501100011033 and the "European Union NextGenerationEU/PRTR". B. Domínguez thanks the Spanish Ministry of Science and Innovation for a predoctoral grant (PREP2022-000687). CEAM is partially supported by GVA.

T. Gómez and M.L. Martínez are acknowledged for their work.

Appendix A. Supplementary data

Supplementary data to this article can be found online at https://doi.org/10.1016/j.atmosres.2025.108239.

Data availability

Data will be made available on request.

References

Bond, T.C., Doherty, S.J., Fahey, D.W., Forster, P.M., Berntsen, T., DeAngelo, B.J., Flanner, M.G., Ghan, S., Kärcher, B., Koch, D., Kinne, S., Kondo, Y., Quinn, P.K., Sarofim, M.C., Schultz, M.G., Schulz, M., Venkataraman, C., Zhang, H., Zhang, S., Bellouin, N., Guttikunda, S.K., Hopke, P.K., Jacobson, M.Z., Kaiser, J.W., Klimont, Z., Lohmann, U., Schwarz, J.P., Shindell, D., Storelvmo, T., Warren, S.G., Zender, C.S., 2013. Bounding the role of black carbon in the climate system: a scientific assessment. J. Geophys. Res. Atmos. 118, 5380–5552. https://doi.org/10.1002/jgrd.50171.

Caponi, L., Formenti, P., Massabó, D., Di Biagio, C., Cazaunau, M., Pangui, E., Chevaillier, S., Landrot, G., Andreae, M.O., Kandler, K., Piketh, S., Saeed, T., Seibert, D., Williams, E., Balkanski, Y., Prati, P., Doussin, J.-F., 2017. Spectral- and size-resolved mass absorption efficiency of mineral dust aerosols in the shortwave spectrum: a simulation chamber study. Atmos. Chem. Phys. 17, 7175–7191. https://doi.org/10.5194/acp-17-7175-2017.

Chakrabarty, R.K., Moosmüller, H., Chen, L.W.A., Lewis, K., Arnott, W.P., Mazzoleni, C., Dubey, M.K., Wold, C.E., Hao, W.M., Kreidenweis, S.M., 2010. Brown carbon in tar balls from smoldering biomass combustion. Atmos. Chem. Phys. 10, 6363–6370. https://doi.org/10.5194/acp-10-6363-2010.

Chen, J., Li, C., Ristovski, Z., Milic, A., Gu, Y., Islam, M.S., Wang, S., Hao, J., Zhang, H., He, C., Guo, H., Fu, H., Miljevic, B., Morawska, L., Thai, P., Lam, Y.F., Pereira, G., Ding, A., Huang, X., Dumka, U.C., 2017. A review of biomass burning: emissions and impacts on air quality, health and climate in China. Sci. Total Environ. 579, 1000–1034. https://doi.org/10.1016/j.scitotenv.2016.11.025.

Chiari, M., Yubero, E., Calzolai, G., Lucarelli, F., Crespo, J., Galindo, N., Nicolás, J.F., Giannoni, M., Nava, S., 2018. Comparison of PIXE and XRF analysis of airborne particulate matter samples collected on Teflon and quartz fibre filters. Nucl. Instrum. Meth. Phys. Res. B 417, 128–132. https://doi.org/10.1016/j.nimb.2017.07.031.

Feng, Y., Ramanathan, V., Kotamarthi, V.R., 2013. Brown carbon: a significant atmospheric absorber of solar radiation? Atmos. Chem. Phys. 13, 8607–8621. https://doi.org/10.5194/acp-13-8607-2013.

Food and Agriculture Organization of the United Nations, 2018. FAO Rice Market Monitor, Volume XXI. N° 1. Available online: https://www.fao.org/home/es/.

Galindo, N., Yubero, E., Nicolás, J.F., Varea, M., Crespo, J., 2018. Characterization of metals in PM_1 and PM_{10} and health risk evaluation at an urban site in the western Mediterranean. Chemosphere 201, 243–250. https://doi.org/10.1016/j.chemosphere.2018.02.162.

Galindo, N., Yubero, E., Clemente, Á., Nicolás, J.F., Varea, M., Crespo, J., 2020. PM events and changes in the chemical composition of urban aerosols: a case study in the western Mediterranean. Chemosphere 244, 125520. https://doi.org/10.1016/j.chemosphere.2019.125520.

Gao, Y., Wang, Q., Li, L., Dai, W., Yu, J., Ding, L., Li, J., Xi, B., Ran, W., Han, Y., Cao, J., 2022. Optical properties of mountain primary and secondary brown carbon aerosols in summertime. Sci. Total Environ. 806, 150570. https://doi.org/10.1016/j.scitotenv.2021.150570.

Giannoni, M., Calzolai, G., Chiari, M., Lucarelli, F., Mazzinghi, A., Nava, S., Ruberto, C., 2015. Feasibility study of ED-XRF analysis of atmospheric particulate matter samples collected with high time resolution. X-Ray Spectrom. 44, 282–288. https://doi.org/10.1002/xrs.2620.

Gilardoni, S., Massoli, P., Paglione, M., Giulianelli, L., Carbone, C., Rinaldi, M., Decesari, S., Sandrini, S., Costabile, F., Gobbi, G.P., Pietrogrande, M.C., Visentin, M., Scotto, F., Fuzzi, S., Facchini, M.C., 2016. Direct observation of aqueous secondary organic aerosol from biomass burning emissions. Proc. Natl. Acad. Sci. USA 113, 10013–10018. https://doi.org/10.1073/pnas.1602212113.

Gilardoni, S., Massoli, P., Marinoni, A., Mazzoleni, C., Freedman, A., Lonati, G., De Iuliis, S., Gianelle, V., 2020. Spatial and temporal variability of carbonaceous aerosol absorption in the Po Valley. Aerosol Air Qual. Res. 20, 2624–2639. https://doi.org/10.4209/aaqr.2020.03.0085.

Guinot, B., Cachier, H., Oikonomou, K., 2007. Geochemical perspectives from a new aerosol chemical mass closure. Atmos. Chem. Phys. 7, 1657–1670. https://doi.org/10.5194/acp-7-1657-2007.

Kaskaoutis, D.G., Grivas, G., Theodosi, C., Tsagkaraki, M., Paraskevopoulou, D., Stavroulas, I., Liakakou, E., Gkikas, A., Hatzianastassiou, N., Wu, C., Gerasopoulos, E., Mihalopoulos, N., 2020. Carbonaceous aerosols in contrasting atmospheric environments in Greek cities: Evaluation of the EC-tracer methods for secondary organic carbon estimation. Atmosphere 11, 161. https://doi.org/10.3390/atmos11020161.

Kaskaoutis, D.G., Grivas, G., Stavroulas, I., Bougiatioti, A., Liakakou, E., Dumka, U.C., Gerasopoulos, E., Mihalopoulos, N., 2021. Apportionment of black and brown carbon spectral absorption sources in the urban environment of Athens, Greece, during winter. Sci. Total Environ. 801, 149739. https://doi.org/10.1016/j.scitotenv.2021.149739.

Koppmann, R., von Czapiewski, K., Reid, J.S., 2005. A review of biomass burning emissions, part I: gaseous emissions of carbon monoxide, methane, volatile organic compounds, and nitrogen containing compounds. Atmos. Chem. Phys. Discuss. 5, 10455–10516. https://doi.org/10.5194/acpd-5-10455-2005.

Laskin, A., Laskin, J., Nizkorodov, S.A., 2015. Chemistry of atmospheric of brown carbon. Chem. Rev. 115, 4335–4382. https://doi.org/10.1021/cr5006167.

Liakakou, E., Kaskaoutis, D.G., Grivas, G., Stavroulas, I., Tsagkaraki, M., Paraskevopoulou, D., Bougiatioti, A., Dumka, U.C., Gerasopoulos, E., Mihalopoulos, N., 2020. Long-term brown carbon spectral characteristics in a Mediterranean city (Athens). Sci. Total Environ. 708, 135019. https://doi.org/10.1016/j.scitotenv.2019.135019.

López-Caravaca, A., Crespo, J., Galindo, N., Yubero, E., Clemente, A., Castañer, R., Nicolás, J.F., 2024. Characterization of water-soluble organic carbon absorption at an urban background site in the South-Eastern Iberian Peninsula. Atmos. Environ. 324, 120435. https://doi.org/10.1016/j.atmosenv.2024.120435.

Nicolás, J.F., Castañer, R., Crespo, J., Yubero, E., Galindo, N., Pastor, C., 2018. Seasonal variability of aerosol absorption parameters at a remote site with high mineral dust loads. Atmos. Res. 210, 100–109. https://doi.org/10.1016/j.atmosres.2018.04.008.

Pani, S.K., Lin, N.-H., Griffith, S.M., Chantara, S., Lee, C.-T., Thepnuan, D., Tsai, Y.I., 2021. Brown carbon light absorption over an urban environment in northern peninsular Southeast Asia. Environ. Pollut. 276, 116735. https://doi.org/10.1016/j.envpol.2021.116735.

Paraskevopoulou, D., Kaskaoutis, D.G., Grivas, G., Bikkina, S., Tsagkaraki, M., Vrettou, I. M., Tavernaraki, K., Papoutsidaki, K., Stavroulas, I., Liakakou, E., Bougiatioti, A., Oikonomou, K., Gerasopoulos, E., Mihalopoulos, N., 2023. Brown carbon absorption and radiative effects under intense residential wood burning conditions in Southeastern Europe: New insights into the abundance and absorptivity of methanol-soluble organic aerosols. Sci. Total Environ. 708, 160434. https://doi.org/10.1016/j.scitotenv.2022.160434.

Park, S., Son, S.-C., Lee, S., 2018. Characterization, sources, and light absorption of fine organic aerosols during summer and winter at an urban site. Atmos. Res. 213, 370–380. https://doi.org/10.1016/j.atmosres.2018.06.017.

Pérez-Landa, G., Ciais, P., Sanz, M.J., Gioli, B., Miglietta, F., Palau, J.L., Gangoiti, G., Millan, M.M., 2007. Mesoscale circulations over complex terrain in the Valencia coastal region, Spain, part 1: simulation of diurnal circulation regimes. Atmos. Chem. Phys. 7, 1835–1849. https://doi.org/10.5194/acp-7-1835-2007.

Rovira, J., Savadkoohi, M., Chen, G.I., Močnik, G., Aas, W., Alados-Arboledas, L., Artiñano, B., Aurela, M., Backman, J., Banerji, S., Beddow, D., Brem, B., Chazeau, B., Coen, M.C., Colombi, C., Conil, S., Costabile, F., Coz, E., de Brito, J.F., Eleftheriadis, K., Favez, O., Flentje, H., Freney, E., Gregorič, A., Gysel-Beer, M., Harrison, R., Hueglin, C., Hyvärinen, A., Ivančič, M., Kalogridis, A.-C., Keernik, H., Konstantinos, G., Laj, P., Liakakou, E., Lin, C., Listrani, S., Luoma, K., Maasikmets, M., Manninen, H.E., Marchand, N., dos Santos, S.M., Mbengue, S., Mihalopoulos, N., Nicolae, D., Niemi, J.V., Norman, M., Ovadnevaite, J., Petit, J.-E., Platt, S., Prévôt, A.S.H., Pujadas, M., Putaud, J.-P., Riffault, V., Rigler, M., Rinaldi, M., Schwarz, J., Silvergren, S., Teinemaa, E., Teinilä, K., Timonen, H., Titos, G., Tobler, A., Vasilescu, J., Vratolis, S., Yttri, K.-E., Yubero, E., Zíková, N., Alastuey, A., Petäjä, T., Querol, X., Yus-Díez, J., Pandolfi, M., 2025. A European aerosol phenomenology – 9: Light absorption properties of carbonaceous aerosol particles across surface Europe. Environ. Int. 195, 109185. https://doi.org/10.1016/j.envint.2024.109185.

Saleh, R., Hennigan, C., McMeeking, G., Chuang, W., Robinson, E., Coe, H., Donahue, N. M., Robinson, A.L., 2013. Absorptivity of brown carbon in fresh and photo-chemically aged biomass-burning emissions. Atmos. Chem. Phys. 13, 7683–7693. https://doi.org/10.5194/acp-13-7683-2013.

Sandradewi, J., Prevot, A.S.H., Szidat, S., Perron, N., Alfarra, L.M., Lanz, V.A., Weingartner, E., Baltensperger, U., 2008. Using aerosol light absorption measurements for the quantitative determination of wood burning and traffic emission contributions to particulate matter. Environ. Sci. Technol. 42, 3316–3323. https://doi.org/10.1021/es702253m.

Savadkoohi, M., Pandolfi, M., Reche, M.C., Niemi, J.V., Mooibroek, D., Titos, G., Green, D.C., Tremper, A.H., Hueglin, C., Liakakou, E., Mihalopoulos, M., Stavroulas, I., Artiñano, B., Coz, E., Alados-Arboledas, L., Beddows, D., Riffault, V., De Brito, J.F., Bastian, S., Baudic, A., Costabile, F., Chazeau, B., Gómez-Amo, J.L., Estellés, V., Matos, V., van der Gaag, E., Gille, G., Luoma, K., Manninen, H.E., Norman, M., Silvergren, S., Petit, J.-E., Putaud, J.-P., Rattigan, O.V., Timonen, H., Tuch, T., Merkel, M., Weinhold, K., Vratolis, S., Vasilescu, J., Favez, O., Harrison, R. M., Lag, P., Wiedensohler, A., Hopke, P.H., Petäjä, T., Querol, X., 2023. The variability of mass concentrations and source apportionment analysis of equivalent black carbon across urban Europe. Environ. Int. 178, 108081. https://doi.org/10.1016/j.envint.2023.108081.

Schuster, G.L., Dubovik, O., Holben, B.N., 2006. Angstrom exponent and bimodal aerosol size distributions. J. Geophys. Res. 111 (D07207). https://doi.org/10.1029/2005JD006328.

Shen, Z., Zhang, Q., Cao, J., Zhang, L., Lei, Y., Huang, Y., Huang, R.J., Gao, J., Zhao, Z., Zhu, C., Yin, X., Zheng, C., Xu, H., Liu, S., 2017. Optical properties and possible sources of brown carbon in $PM_{2.5}$ over Xi'an, China. Atmos. Environ. 150, 322–330. https://doi.org/10.1016/j.atmosenv.2016.11.024.

Sheoran, R., Dumka, U.C., Kaskaoutis, D.G., Grivas, G., Ram, K., Prakash, J., Hooda, R.K., Tiwari, R.K., Mihalopoulos, N., 2021. Chemical composition and source apportionment of total suspended particulate in the Central Himalayan Region. Atmosphere 12, 1228. https://doi.org/10.3390/atmos12091228.

Sigsgaard, T., Forsberg, B., Annesi-Maesano, I., Blomberg, A., Bølling, A., Boman, C., Bønløkke, J., Brauer, M., Bruce, N., Héroux, M.-E., Hirvonen, M.-R., Kelly, F., Künzli, N., Lundbäck, B., Moshammer, H., Noonan, C., Pagels, J., Sallsten, G., Sculier, J.-P., Brunekreef, B., 2015. Health impacts of anthropogenic biomass burning in the developed world. Eur. Respir. J. 46, 1577–1588. https://doi.org/10.1183/13993003.01865-2014.

Torregrosa, A., Giner, J.M., Velázquez-Martí, B., 2021. Equipment performance, costs and constraints of packaging and transporting rice straw for alternative uses to burning in the "Parc Natural l'Albufera de València" (Spain). Agriculture 11, 570. https://doi.org/10.3390/agriculture11060570.

Turpin, B.J., Huntzicker, J.J., 1995. Identification of secondary Organic Aerosol Episodes and Quantitation of primary and secondary Organic Aerosol Concentrations during SCAQS. Atmos. Environ. 29, 3527–3544. https://doi.org/10.1016/1352-2310(94)00276-Q.

Van Den Heuvel, R., Staelens, J., Koppen, G., Schoeters, G., 2018. Toxicity of urban PM_{10} and relation with tracers of biomass burning. Int. J. Environ. Res. Public Health 15, 320. https://doi.org/10.3390/ijerph15020320.

Viana, M., López, J.M., Querol, X., Alastuey, A., García-Gacio, D., Blamco-Heras, G., López-Mahia, P., Piñeiro-Iglesias, M., Sanz, M.J., Sanz, F., Chi, X., Maenhaut, W., 2008. Tracers and impact of open burning of rice straw residues on PM in Eastern Spain. Atmos. Environ. 42, 1941–1957. https://doi.org/10.1016/j.atmosenv.2007.11.012.

Wang, Q., Han, Y., Ye, J., Liu, S., Pongpiachan, S., Zhang, N., Han, Y., Tian, J., Wu, C., Zhang, Q., Zhang, W., Zhao, Z., Cao, J., 2019. High contribution of secondary brown carbon to aerosol light absorption in the southeastern margin of Tibetan Plateau. Geophys. Res. Lett. 46, 4962–4970. https://doi.org/10.1029/2019GL082731.

Wang, Q., Wang, L., Li, X., Xin, J., Liu, Z., Sun, Y., Liu, J., Zhang, Y., Du, W., Jina, X., Zhang, T., Liu, S., Liu, Q., Chen, J., Cheng, M., Wang, Y., 2020. Emission characteristics of size distribution, chemical composition and light absorption of particles from field-scale crop residue burning in Northeast China. Sci. Total Environ. 710, 136304. https://doi.org/10.1016/j.scitotenv.2019.136304.

Washenfelder, R.A., Attwood, A.R., Brock, C.A., Guo, H., Xu, L., Weber, R.J., Ng, N.L., Allen, H.M., Ayres, B.R., Baumann, K., Cohen, R.C., Draper, D.C., Duffey, K.C., Edgerton, E., Fry, J.L., Hu, W.W., Jimenez, J.L., Palm, B.B., Romer, P., Stone, E.A., Wooldridge, P.J., Brown, S.S., 2015. Biomass burning dominates brown carbon absorption in the rural Southeastern United States. Geophys. Res. Lett. 42, 653–664. https://doi.org/10.1002/2014GL062444.

Wu, C., Yu, J.Z., 2016. Determination of primary combustion source organic carbon-to-elemental carbon (OC/EC) ratio using ambient OC and EC measurements: secondary OC-EC correlation minimization method. Atmos. Chem. Phys. 16, 5453–5465. www.atmos-chem-phys.net/16/5453/2016/.

Wu, C., Wu, D., Yu, J.Z., 2018. Quantifying black carbon light absorption enhancement with a novel statistical approach. Atmos. Chem. Phys. 18, 289–309. https://doi.org/10.5194/acp-18-289-2018.

Wu, C., Wu, D., Yu, J.Z., 2019. Estimation and uncertainty analysis of secondary organic carbon using 1 year of hourly organic and elemental carbon data. J. Geophys. Res. 124, 2774–2795. https://doi.org/10.1029/2018JD029290.

Wu, C., He, C., Brown, Z.E., Miljevic, B., Zhang, C., Wang, H., Wang, B., Morawska, L., Ristovski, Z., 2023. Light absorption properties of black and brown carbon during the prescribed burning season at an urban background site in Brisbane, Australia. Atmos. Environ. 313, 120072. https://doi.org/10.1016/j.atmosenv.2023.120072.

Xu, B., Fan, M., Lu, X., Zhang, Z., Li, M., Tao, J., Chen, L., Son, S., 2024. Light absorption properties and source contributions of black and brown carbon in Guangxi, southern China. Atmos. Res. 302, 107317. https://doi.org/10.1016/j.atmosres.2024.107317.

Zhang, Y., Albinet, A., Petit, J.E., Jacob, V., Chevrier, F., Gille, G., Pontet, S., Chrétien, E., Dominik-Sègue, M., Levigoureux, G., Močnik, G., Gros, V., Jaffrezo, J.-L., Favez, O., 2020. Substantial brown carbon emissions from winter residential wood burning over France. Sci. Total Environ. 743, 140752. https://doi.org/10.1016/j.scitotenv.2020.140752.

Zhu, C.-S., Qu, Y., Huang, H., Chen, J., Dai, W.-T., Huang, R.-J., Cao, J.-J., 2021. Black carbon and secondary brown carbon, the dominant light absorption and direct radiative forcing contributors of the atmospheric aerosols over the Tibetan Plateau. Geophys. Res. Lett. 48. https://doi.org/10.1029/2021GL092524 e2021GL092524.